THE DISTRIBUTION OF LINEAR POLARIZATION OVER 13 EXTENDED SOURCES AT 21·2 CM WAVELENGTH

By D. Morris* and J. B. Whiteoak*

[*Manuscript received February* 8, 1968]

Summary

The distribution of linear polarization over 13 bright radio sources has been determined at 21 cm wavelength with an east–west interferometer. The results are presented in the form of strip brightness distributions of polarized flux and direction of polarization, with a resolution of 1′ by 20′. It is suggested that axial rotation during evolution contributes to the observed polarization features of extended radio sources.

I. Introduction

Observations of the distribution of linear polarization over radio sources, particularly if obtained at more than one wavelength, help to trace their evolution by providing information about the magnetic field configurations and associated internal mass motions and depolarization mechanisms. At present, data are available for only those sources that can be resolved by single antennas and for a few additional bright sources observed by interferometer techniques. With regard to the latter group, the work of Seielstad (1967) at 10·6 cm is the most comprehensive and also contains a summary of previous investigations. The observations to be described here form the initial observations taken to provide comparable data at 21 cm, and to extend the programme to sources at southern declinations.

Thirteen radio sources identified with galaxies and containing multiple components were studied using the east–west baseline of the interferometer at Parkes. The measured Fourier transforms of the Stokes parameters Q and U were inverted by an approximate method to yield strip scans across each source with an effective resolution of approximately 1′ by 20′. The choice of sources was confined to those that are appreciably resolved by a beam of half-power width 1′ and have an integrated polarized flux density of at least 0·5 f.u.† at 21 cm wavelength.

II. Equipment

The interferometer has been described by Cole (1967) and Batchelor, Cole, and Shimmins (1968). The collecting elements consist of the 210 ft radio telescope and a 60 ft parabola mounted on railway tracks which run from separations of 400 ft to 1400 ft in north–south and east–west directions. Both telescopes have altazimuth mountings, the pointing of the 60 ft telescope being slaved to the 210 ft one. As a consequence of this type of mounting, position angle (i.e. orientation with respect to celestial coordinates) is related to feed orientation through the parallactic angle.

* Division of Radiophysics, CSIRO, P.O. Box 76, Epping, N.S.W. 2121.

† 1 flux unit = $10^{-26}\,\mathrm{W\,m^{-2}\,Hz^{-1}}$.

Two servo systems driven from the "master equatorial" system of the 210 ft telescope constrained the orientation of the feeds to a selected position angle. Although the absolute accuracy of the servo control was about 1°, the relative orientation of the two feeds could be maintained to a higher accuracy. The zero point of the position angle scale was ascertained by radiating a linearly polarized signal from the apex of the 210 ft paraboloid. The receivers used identical crystal mixers without image rejection and were operated with a 1412 MHz local oscillator. The i.f. bandwidth was 10 MHz.

The factors contributing to the instrumental polarization and their removal have been described by Seielstad (1967). At Parkes, in preliminary observations using double-dipole primary feeds, the instrumental circular polarization was 2% on-axis, increasing to as much as 15% off-axis. However, an acceptable performance was obtained by using a hybrid-mode horn (Minnett and Thomas 1966) to illuminate the 210 ft antenna, and a cylindrical horn with surrounding chokes (von Geyer 1966) for the smaller telescope. The desirable characteristics of the hybrid-mode horn are a circularly symmetric beam and a polarization that is linear and constant in direction over the entire aperture of the telescope. In principle there are no cross-polarized side lobes. In contrast to conventional feeds, for which the overall linear polarization of the telescope depends on the cancellation of contributions with different polarizations from different sectors of the antenna surface, the overall polarization is less sensitive to surface irregularities and their variation with zenith angle. The design of the particular feeds used was effected by Dr. B. McA. Thomas of the Division of Radiophysics, CSIRO. The residual instrumental circular polarization was further reduced by appropriate adjustment of the feed ellipticity. For this purpose, the hybrid-mode feed contained orthogonal probes. One of these supplied the receiver directly; the other fed the receiver through a line-stretcher, variable attenuator, and directional coupler. By adjustment of these components during observations of the Orion Nebula, the residual instrumental circular polarization was reduced to 0·74%.

The resulting characteristics of the interference polarimeter are shown in Figure 1; (*a*) shows the variation in offset (F.A.(60)—F.A.(210)) required for oppositely polarized telescopes as a function of feed orientation of the 210 ft telescope, while (*b*) similarly shows the variation in instrumental circular polarization (the residual fringe for the appropriate offset). The deviation from orthogonality in the scale readings and the variation of the offset reflect instrumental linear polarization together with any dial errors (Morris, Radhakrishnan, and Seielstad 1964). The variation is sufficiently slow with feed angle for corrections to be applied during the observations. The primary beam patterns with parallel and orthogonal feeds are shown in Figure 2. Figure 2(*b*) shows the changes in the instrumental circular polarization during two scans in right ascension across M87 taken with the feeds set orthogonal at position angles of 0° and 90° approximately. One scan (solid curve) was taken through the position of the source, the other (dashed curve) at the declination where the maximum responses in the cross-polarized side lobes are located. It can be seen that at no position does the response exceed 2% of the response with parallel feeds on-axis. No detectable variation in these characteristics occurred with zenith angle.

III. Observations

The theory and assumptions underlying the techniques used have been described in detail by Seielstad (1967). The linear polarization distribution was initially derived in terms of the brightness distributions for the Stokes parameters I (the total flux density), Q ($= I_p \cos 2\theta$, where I_p is the polarized flux density and θ the position angle of polarization), and U ($= I_p \sin 2\theta$). The fourth parameter V (representing circular polarization) was assumed to be zero. The interferometer

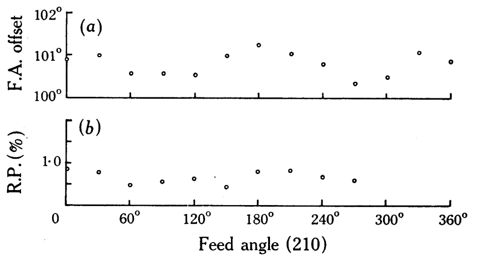

Fig. 1.—Variation with feed angle of the 210 ft telescope for (a) the offset of the feed orientation of the 60 ft telescope to produce feed orthogonality, and (b) the residual polarization (R.P.) with orthogonal feeds.

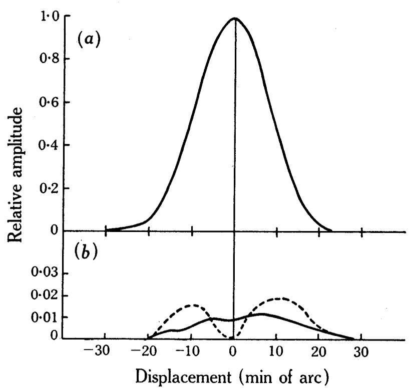

Fig. 2.—Primary beam shapes of the interferometer with (a) parallel feeds and (b) orthogonal feeds. The dashed curve in (b) represents a scan taken off-source showing the maximum contributions from cross-polarized side lobes.

observations yielded the Fourier transforms of these parameters. Complete restoration of the observations to brightness distributions requires absolute phase as well as amplitude information for I, Q, and U at each antenna spacing. Since the Parkes interferometer was neither phase-stable nor accurately surveyed, only measurements of the phases of Q and U relative to $I+Q$ could be made.

Each source was observed at a series of antenna spacings separated by 100 or 200 ft. If possible, the time of observation was usually chosen so that the projected baseline of the interferometer was parallel to either the major or minor axis of the source. At each separation four measurements were made. Firstly, $\frac{1}{2}(I+Q)$ was observed, with the position angles of both feeds equal to the direction of integrated polarization (as given by single-dish observations and listed in Table 1). The quantity $\frac{1}{2}U$ was then observed by rotating the feed of the 60 ft telescope in a positive sense to its orthogonal position. Further rotation of both feeds through $+45°$ in the same direction yielded observations of the quantity $\frac{1}{2}Q$. The fourth and final observation consisted of a repetition of the first. In theory, the chosen frame of reference for the Stokes vectors is such that the zero-spacing value of U is zero, while that of Q is the integrated polarized flux (Morris, Radhakrishnan, and Seielstad 1964). In practice, however, ionospheric Faraday rotation caused a small rotation of this frame of reference. With a receiver time constant of 1 sec, the natural fringes were recorded on paper tape at half-second intervals. The observations of U and Q generally extended over 3 or 4 min; somewhat smaller times were used for $I+Q$. All subsequent reductions were effected with a CDC 3200 computer. For each observation, values of fringe amplitude and phase were calculated by the method of least squares. The relative phases of U and Q were determined by interpolation between the phases of the first and fourth observation at each spacing. At this stage, corrections for signal attenuation due to the receiver time constant were applied.

The observation of PKS 1226+02 with parallel feeds confirmed that the variation of the interferometer gain with antenna separation was negligible. A flux density calibration was provided by observation of PKS 0521−36, which was assumed to have a flux density of 16 f.u. at 21 cm.

IV. Results

The sources observed and relevant polarization data are listed in Table 1. Most of the columns are self-explanatory. The polarization data in the first columns were obtained with a single dish and were used as zero-spacing information. The last column contains the calculated Faraday rotation due to the ionosphere at the time of observation. The calculations are based on $f_0 F_2$ data supplied by the Ionospheric Prediction Service and assume a thin uniform slab as a model for the ionosphere (Roberts and Komesaroff 1965, p. 138).

Table 2 contains the measured fringe amplitudes (in flux units) and relative phases (in degrees). For each measurement the baseline parameters, i.e. the length S in wavelengths and position angle P.A. of the projected baseline at the source position are shown. The sign convention of the phases is such that a positive value corresponds to an apparent displacement to greater right ascensions (in accordance with the conventions of Fomalont (1976*a*) and Seielstad (1967)). The errors quoted are standard deviations derived from the least squares programme that was used to derive the amplitudes and phases. Additional errors in phase due to inaccuracy in interpolation may amount to $\pm 20°$. The values adopted for zero antenna spacing contained an allowance for ionospheric Faraday rotation. As an illustration, Figure 3 shows the result for the source PKS 0043−42.

Only for PKS 1648+05, where the percentage polarization is low, have corrections for a constant instrumental circular polarization ($0\cdot74\%$) been included. The correction was regarded as unnecessary in all other cases.

(*a*) *Approximate Inversion of Visibility Functions*

Rather than fit models to the observations, with the disadvantage of requiring certain assumptions regarding basic model shapes, approximate one-dimensional brightness distributions of $I+Q$, U, and Q were calculated by Fourier inversion, following the method of Fomalont (1967*b*). These enabled the distribution of polarized flux density and polarization direction to be derived. For such a technique, absolute phases for the observations are necessary. It was assumed that the phase of $I+Q$ was not significantly dependent on the Q contribution, so that the results of other observers, which in general are for some combination of both U and Q, could be used. It was possible to interpolate between the observations of Fomalont (1967*a*) when the present results were obtained with a projected baseline directed

TABLE 1

ASSUMED SOURCE PARAMETERS

PKS Source No.	Brightness Temp.* (10^3 °K)	Polarization (%) at 21·5 cm†	Position Angle (°) at 21·5 cm†	Major Axis‡ (°)	Intrinsic Angle§ (°)	Flux Density‖ (f.u.)	Faraday Rotation¶ (°)
0043−42	2·5	9·8±0·6	137±2	136±2	136±2	8·1	6·3
0106+13	12	8·2±0·3	58±3	20±8	91±2	15·5	7·3
0356+10	1·0	6·0±0·6	74±5	25±10	50±6	11·7	6·8
0518−45	0·9	3·1±0·4	50±5	105±2	104±4	71·8	4·0
0618−37	1·0	14·0±4·3	71±6	84±4	69±3	3·0	3·1
0945+07	1·6	5·5±0·4	136±2	90±10	160±6	8·5	6·5
1216+06	0·6	7·7±0·3	118±3	85±7	94±2	18	3·0
1322−42	4·5	7·0±0·5	175±3	46·5±2	147±3	288	2·0
1559+02	1·4	6·0±0·9	2±5	90	156±5	7·4	3·3
1648+05	19	0·9±0·2	41±2	100±2	28±3	46	4·1
1717−00	6·1	2·9±0·3	167±2	90	82±8	50	7·2
2152−69	5·0	2·7±0·2	116±4	96±10	32±3	32	3·3
2356−61	2·5	4·9±0·3	66±2	132±2	7±5	23	6·6
0521−36		Flux calibration				16·0	

* Morris and Berge (1964) and Ekers (1967).

† Gardner and Davies (1966*b*).

‡ Maltby and Moffet (1962) and Ekers (1967).

§ Gardner and Davies (1966*a*).

‖ At 21 cm from the Parkes catalogue of radio sources.

¶ Calculated from data from the Ionospheric Prediction Service.

near position angle 90°. For sources not observed by Fomalont, absolute phases of $I+Q$ were calculated from the models of Ekers (1967), or in the case of PKS 0106+13 from a simple model composed of Gaussian components. For Ekers's models, the sign of the calculated phase is not known, and both senses were tried in the inversions. Only one sense is shown in the figures, since the changes produced by sign reversal were small. In the case of PKS 2356−61, the assumed model is symmetrical and the resultant phase is either ±180° or 0°. Naturally, the uncertainties in the derived brightness distributions are larger when models are used to calculate the phases. For each inversion it was assumed that all the observations were made at a constant direction of projected baseline. In reality, observations were taken over a period of time during which this direction varied continuously. The effect of this variation is not too important when the position angle is aligned along the major axis of the

TABLE 2

OBSERVED VALUES OF FRINGE AMPLITUDE AND RELATIVE PHASE

(1)	(2)	(3)	(4)	(5)	(6)	(7)	(8)	(9)	(10)	(11)
Parallel Feeds			Orthogonal Feeds							
S (λ)	P.A. (°)	$I+Q$ (f.u.)	S (λ)	P.A. (°)	U (f.u.)	$\Delta\phi(U)$ (°)	S (λ)	P.A. (°)	Q (f.u.)	$\Delta\phi(Q)$ (°)
PKS 0043−42										
0	—	9·1±0·5	0	—	0·21±0·06	—	0	—	0·96±0·1	—
403	153	6·2±0·4	400	155	0·34±0·05	50±8	397	157	0·83±0·08	346±6
511	146	4·9±0·12	508	147	0·21±0·04	22±10	503	149	0·95±0·06	1±3
636	140	4·1±0·13	631	141	0·18±0·06	345±21	624	143	0·81±0·04	3±4
783	134	2·7±0·14	777	135	0·18±0·12	275±40	768	136	0·44±0·06	24±9
953	125	1·6±0·14	947	126	0·05±0·05	299±62	937	128	0·28±0·04	41±11
1116	121	1·2±0·13	1108	122	0·15±0·07	238±28	1099	123	0·17±0·04	108±18
1278	116	1·8±0·12	1271	117	0·14±0·05	287±23	1261	118	0·23±0·05	137±13
1440	113	2·5±0·13	1434	113	0·15±0·15	37±58	1425	114	0·11±0·06	93±28
1578	109	2·8±0·1	1572	110	0·10±0·20	—	1563	111	0·12±0·13	—
1732	106	3·1±0·6	1727	106	0·21±0·07	7±26	1718	107	0·07±0·07	212±58
1877	102	2·7±0·1	1873	103	0·07±0·21	—	1865	104	0·16±0·16	—
PKS 0106+13 (3C 33)										
0	—	14·2±0·09	0	—	0·24±0·08	180	0	—	0·95±0·09	360
472	77	9·8±0·2	466	77	0·29±0·06	195±10	457	76	0·77±0·05	342±10
601	79	8·2±0·1	596	79	0·22±0·05	150±12	588	79	0·77±0·05	338±11
761	81	6·8±0·1	750	80	—	—	739	80	—	—
921	83	5·3±0·1	914	82	0·29±0·04	206±10	906	82	0·65±0·05	6±12
1104	85	4·4±0·1	1093	84	—	—	1081	84	0·57±0·06	5±15
1275	86	4·8±0·1	1270	86	0·42±0·05	199±8	1263	86	0·73±0·09	25±10
1424	87	3·9±0·1	1420	87	0·44±0·11	148±16	1416	87	0·66±0·05	354±16
1574	89	5·4±0·4	1573	88	0·40±0·08	175±15	1571	88	0·77±0·05	2±8
1895	91	5·9±0·1	1899	91	0·31±0·08	—	1904	91	0·87±0·06	—
PKS 0356+10 (3C 98)										
0	—	11·7±0·7	0	—	0·16±0·06	180	0	—	0·65±0·06	360
432	77	7·1±0·2	428	77	0·20±0·05	152±14	421	77	0·30±0·06	10±12
621	80	5·1±0·1	615	80	0·48±0·09	176±10	603	79	0·11±0·07	—
832	82	2·5±0·1	825	82	0·51±0·05	147±6	811	81	0·16±0·05	11±18
1041	83	1·2±0·1	1032	83	0·47±0·05	95±10	1018	83	0·10±0·05	20±20
1248	85	2·0±0·2	1241	85	0·52±0·05	—	1228	85	0·23±0·05	—
1465	86	3·2±0·1	1460	86	0·49±0·05	30±7	1447	85	0·16±0·06	309±20
1686	87	3·9±0·1	1678	87	0·43±0·06	24±8	1666	87	0·16±0·08	354±25
1919	88	4·2±0·1	1916	88	0·47±0·09	60±12	1908	88	0·13±0·06	10±27
PKS 0518–45 (Pictor A): Scan 1										
0	—	71·8±4·0	0	—	0·42±0·2	360	0	—	2·2±0·3	360
458	26	41·0±1·0	459	27	1·3±0·07	0±5	462	28	3·2±0·1	330±5
673	30	23·2±0·3	676	31	1·4±0·06	12±6	679	32	2·5±0·08	272±8
921	35	2·7±0·5	925	36	1·0±0·07	189±11	930	37	1·5±0·08	67±12
1161	39	15·5±0·3	1166	40	0·66±0·06	150±6	1172	41	2·3±0·07	4±6
1419	43	4·9±0·1	1423	44	0·88±0·07	195±12	1429	45	0·71±0·17	57±5
1610	47	14·6±0·3	1615	47	1·27±0·06	196±5	1622	48	0·72±0·08	292±5
PKS 0518–45 (Pictor A): Scan 2										
0	—	71·8±4	0	—	0·28±0·2	360	0	—	2·2±0·3	360
463	138	11·4±0·2	461	138	0·44±0·05	25±6	457	140	2·6±0·1	343±6
571	133	25·0±0·2	568	134	0·27±0·05	337±8	564	135	2·8±0·1	358±10
721	128	24·5±0·2	717	129	0·56±0·12	270±12	712	130	2·4±0·05	317±11
892	120	7·5±0·2	888	121	0·15±0·05	89±22	883	122	2·8±0·05	305±20
1038	117	15·7±0·2	1034	117	0·27±0·06	206±14	1028	118	3·5±0·05	331±13
1199	113	8·8±0·2	1194	114	0·25±0·06	180±15	1187	115	2·9±0·06	316±14
1350	109	10·4±0·2	1346	110	0·22±0·05	141±13	1339	111	2·3±0·05	19±12
1511	106	15·7±0·2	1507	107	0·07±0·07	195±20	1500	108	2·8±0·25	355±20

TABLE 2 (*Continued*)

(1)	(2)	(3)	(4)	(5)	(6)	(7)	(8)	(9)	(10)	(11)
Parallel Feeds			Orthogonal Feeds							
S (λ)	P.A. (°)	$I+Q$ (f.u.)	S (λ)	P.A. (°)	U (f.u.)	$\Delta\phi(U)$ (°)	S (λ)	P.A. (°)	Q (f.u.)	$\Delta\phi(Q)$ (°)
PKS 0618–37										
0	—	3·0±0·2	0	—	0·05±0·03	180	0	—	0·42±0·05	360
504	115	2·5±0·08	500	116	0·12±0·06	115±30	495	117	0·17±0·05	4±25
753	111	2·0±0·11	748	112	0·20±0·05	103±13	742	113	0·28±0·05	19±12
1056	107	1·4±0·11	1050	108	0·12±0·07	40±32	1042	109	0·19±0·05	357±30
1292	103	0·61±0·10	1286	104	0·14±0·06	285±25	1279	105	0·07±0·05	220±40
1452	100	0·31±0·12	1445	101	0·16±0·06	300±40	1438	102	0·09±0·04	283±45
1619	97	0·54±0·09	1615	98	0·07±0·07	289±50	1609	98	0·04±0·05	229±54
1776	94	0·77±0·1	1773	94	0·10±1·0	—	1769	95	0·05±0·10	—
1929	91	1·13±0·1	1928	91	0·10±0·20	—	1926	92	0·04±0·12	—
PKS 0945+07 (3C 227)										
0	—	8·5±0·5	0	—	0·11±0·05	180	0	—	0·47±0·06	360
534	92	2·9±0·10	538	92	0·11±0·04	142±30	548	92	0·20±0·06	71±25
628	84	1·7±0·11	622	84	—	—	607	93	0·22±0·04	—
768	92	1·26±0·13	773	92	0·23±0·04	55±15	783	92	0·31±0·04	66±10
903	85	1·64±0·09	928	85	—	—	916	85	—	—
1071	92	2·92±0·12	1077	92	0·19±0·05	32±14	1087	92	0·42±0·10	26±16
1259	87	2·9±0·12	1254	87	0·16±0·10	342±35	1242	87	—	—
1379	91	1·94±0·13	1385	91	0·04±0·08	—	1398	87	0·35±0·05	—
1583	89	0·72±0·12	1581	89	0·12±0·05	344±20	1576	88	0·35±0·05	328±18
1695	91	0·46±0·10	1701	91	0·24±0·05	294±25	1710	90	0·35±0·06	260±20
1944	90	1·85±0·13	1946	90	0·17±0·04	268±18	1949	90	0·18±0·05	282±14
PKS 1226+06 (3C 270): Scan 1										
0	—	18·1±0·9	0	—	0·16±0·06	180	0	—	1·39±0·06	360
423	81	2·0±0·1	418	81	0·22±0·06	158±20	409	81	0·35±0·05	137±11
637	83	6·7±0·1	630	83	0·54±0·06	306±7	619	83	0·42±0·05	—
838	84	4·1±0·1	830	84	0·41±0·06	317±9	818	84	0·35±0·05	313±8
1011	85	1·4±0·11	1002	85	0·24±0·05	50±15	987	85	0·56±0·06	40±10
1189	86	0·93±0·09	1179	86	0·16±0·04	127±20	1167	86	0·38±0·05	142±14
1366	87	0·18±0·11	1358	87	0·04±0·05	—	1345	87	0·14±0·07	—
1544	88	0·64±0·10	1536	88	0·29±0·05	342±17	1524	88	0·23±0·04	186±14
1713	89	0·10±0·13	1709	88	0·27±0·08	83±40	1702	88	0·14±0·08	258±50
1917	89	0·78±0·14	1917	89	0·23±0·06	20±22	1915	89	0·08±0·05	180±22
PKS 1226+06 (3C 270): Scan 2										
0	—	18·1±0·9	0	—	0·13±0·06	180	0	—	1·39±0·06	360
420	81	1·67±0·24	414	81	0·46±0·07	—	406	80	0·26±0·06	—
592	83	6·24±0·15	592	83	—	—	574	82	0·42±0·12	316±16
804	84	4·78±0·12	797	84	0·26±0·05	—	786	84	0·55±0·06	303±6
1110	85	0·84±0·12	1102	85	0·44±0·08	—	1087	85	0·24±0·04	115±15
1282	86	0·23±0·10	1271	86	0·09±0·05	—	1256	86	0·30±0·05	—
1472	87	0·72±0·12	1462	87	0·34±0·09	15±20	1449	86	0·17±0·06	—
1703	87	0·17±0·11	1694	87	0·18±0·10	330±25	1682	87	0·10±0·06	—
1900	88	0·89±0·11	1895	88	0·21±0·04	40±18	1883	88	0·12±0·05	296±50
PKS 1322−42 (Centaurus A): Scan 1										
0	—	288±18	0	—	0·8±0·4	—	0	—	20·1±2·0	360
442	138	195±2	441	139	10·9±0·3	84±3	439	139	19·2±0·3	6±3
581	135	161±3	578	135	9·5±0·3	72±3	576	136	12·7±0·5	2±3
730	132	152±4	727	133	11·6±0·2	72±3	725	133	14·3±0·4	11±3
905	129	118±3	900	130	9·9±0·3	98±3	897	130	13·2±0·2	6±4
1144	127	47±1	1140	127	6·8±0·2	94±3	1136	128	9·4±0·2	32±4
1327	124	9·9±1	1322	125	5·0±0·2	79±7	1318	125	9·3±0·3	2±6
1649	122	21·5±1·3	1644	123	4·9±0·2	14±5	1638	123	5·3±0·2	236±5
1509	120	36·4±	1502	121	6·1±0·2	—	1497	121	6·7±0·1	—

Table 2 (*Continued*)

(1)	(2)	(3)	(4)	(5)	(6)	(7)	(8)	(9)	(10)	(11)
Parallel Feeds					Orthogonal Feeds					
S (λ)	P.A. (°)	$I+Q$ (f.u.)	S (λ)	P.A. (°)	U (f.u.)	$\Delta\phi(U)$ (°)	S (λ)	P.A. (°)	Q (f.u.)	$\Delta\phi(Q)$ (°)
PKS 1322−42 (Centaurus A): Scan 2										
0	—	288±18	0	—	0·8±0·4	180	0	—	20·1±2·0	360
556	106	53·4±1	555	106	8·5±0·2	140±4	554	106	14·2±0·2	16±4
752	104	102±1	750	104	6·6±0·2	75±3	749	104	12·7±0·2	347±3
977	102	79±1	976	102	1·0±1·0	90±10	974	103	10·3±0·1	2±10
1238	100	24±1	1236	100	2·5±0·1	97±3	1234	101	8·7±0·2	327±4
1482	98	41·7±1	1480	99	1·7±0·1	119±4	1479	99	5·8±0·1	114±4
1715	97	22·7±0·08	1713	97	3·6±0·2	205±5	1712	97	6·1±0·2	339±5
1905	95	18·8±0·2	1904	95	1·0±0·1	167±7	1902	96	2·8±0·1	309±8
PKS 1322−42 (Centaurus A): Scan 3										
0	—	288±18	0	—	1·3±0·4	180	0	—	20·1±2·0	360
399	157	96±3	398	158	10·8±0·4	92±4	396	159	12·3±0·4	345±3
495	153	86±1	494	154	11·7±0·1	58±3	492	155	11·3±0·1	334±3
606	150	82±2	604	150	10·5±0·3	83±4	602	151	10·5±0·2	330±4
730	147	76±1·5	727	147	12·3±0·3	55±3	725	148	10·0±0·4	307±3
845	144	82·2±0·9	842	144	11·9±0·3	56±4	839	145	11·3±0·3	321±4
977	141	75·5±0·6	974	141	12·8±0·2	35±3	970	142	10·3±0·1	325±3
1101	138	67·0±1·5	1097	139	12·5±0·2	43±3	1093	139	9·6±0·1	328±4
1233	135	61·9±1·5	1228	140	11·6±0·3	48±5	1224	137	8·3±0·2	320±4
1343	133	46·2±0·4	1338	133	10·8±0·1	50±4	1334	134	7·4±0·2	333±3
1464	131	21·8±0·4	1459	131	7·4±0·1	45±3	1453	132	6·3±0·2	11±3
1580	128	3·6±0·2	1574	129	4·0±0·1	25±4	1569	129	6·3±0·4	321±5
PKS 1559+02 (3C 327a)										
0	—	7·4±0·4	0	—	0·05±0·03	180	0	—	0·44±0·07	348±6
434	89	4·1±0·1	439	89	0·13±0·04	124±16	450	89	0·46±0·05	351±8
552	89	4·0±0·1	558	89	0·24±0·05	103±13	570	89	0·39±0·05	351±8
701	90	5·4±0·2	710	90	0·22±0·05	41±15	722	90	0·43±0·05	340±8
868	90	5·7±0·1	877	90	0·28±0·04	28±9	889	90	0·43±0·04	341±6
1038	90	4·8±0·1	1046	90	0·37±0·05	13±9	1058	90	0·47±0·08	357±7
1220	90	3·6±0·1	1227	90	0·13±0·05	49±20	1238	90	0·38±0·06	15±10
1383	90	2·5±	1389	90	0·25±0·08	14±16	1397	90	0·35±0·06	352±10
1551	90	2·5±0·1	1555	90	0·19±0·07	356±20	1561	90	0·38±0·05	332±8
1715	90	2·5±0·1	1717	90	0·18±0·08	321±21	1719	90	0·35±0·07	320±20
1860	89	2·3±0·13	1859	89	0·37±0·1	330±16	1857	89	0·15±0·17	345±25
PKS 1648+05 (Hercules A)										
0	—	46±3	0	—	0·07±0·05	360	0	—	0·46±0·1	360
497	91	31±1	501	91	0·57±0·05	22±6	508	90	0·75±0·05	41±7
769	91	14±0·5	775	91	0·40±0·06	15±10	784	91	0·72±0·05	33±10
1063	91	14±0·6	1069	91	0·23±0·05	135±15	1081	91	0·43±0·06	89±8
1375	91	25±0·7	1381	91	0·16±0·05	166±22	1392	91	0·44±0·05	11±20
1712	91	28±0·9	1719	90	0·22±0·07	151±40	1727	90	0·26±0·16	28±40
1895	90	26±0·5	1899	90	—	—	1904	90	—	—
PKS 1717−00 (3C 353)										
0	—	50±3	0	—	0·4±0·1	180	0	—	1·6±0·16	360
368	88	30±0·5	362	88	—	—	351	88	—	—
488	88	20±0·5	481	88	—	—	470	88	—	—
640	89	11·5±0·15	633	89	0·69±0·16	279±13	620	89	2·3±0·1	301±12
872	89	13·7±0·2	863	89	1·00±0·08	60±4	836	89	1·60±0·06	109±5
1039	89	18·9±0·2	1033	89	0·97±0·07	129±5	1022	89	1·50±0·05	115±5
1215	89	18·5±0·6	1209	89	1·21±0·08	150±6	1199	89	1·63±0·06	94±5
1360	89	—	1356	89	1·03±0·1	135±6	1347	89	1·52±0·11	—
1556	89	16·3±0·2	1553	89	1·4±0·12	170±5	1545	89	1·29±0·05	89±5
1686	89	15·1±0·2	1684	89	1·2±0·16	102±8	1680	89	1·32±0·08	2±8
1808	89	12·5±0·2	1808	89	0·94±0·16	115±10	1807	89	1·10±0·05	282±10

TABLE 2 (*Continued*)

(1)	(2)	(3)	(4)	(5)	(6)	(7)	(8)	(9)	(10)	(11)
Parallel Feeds			Orthogonal Feeds							
S (λ)	P.A. (°)	$I+Q$ (f.u.)	S (λ)	P.A. (°)	U (f.u.)	$\Delta\phi(U)$ (°)	S (λ)	P.A. (°)	Q (f.u.)	$\Delta\phi(Q)$ (°)
PKS 2152−69 (21−64)										
0	—	2·7±0·2	0	—	0·11±0·05	—	0	—	0·94±0·09	360
582	62	1·81±0·03	582	63	0·77±0·05	305±5	583	64	0·91±0·05	334±4
705	67	1·90±0·2	705	68	0·83±0·05	356±4	705	69	1·46±0·13	30±8
844	71	2·1±0·06	845	72	0·87±0·05	—	845	73	1·29±0·06	—
1000	77	2·2±0·05	1000	78	1·29±0·07	358±5	1001	79	1·45±0·07	1±4
1147	81	2·0±0·05	1147	82	0·97±0·05	10±4	1147	83	1·5±0·06	340±6
1292	85	1·61±0·02	1292	86	0·67±0·06	—	1292	87	—	—
1433	89	1·46±0·03	1433	90	0·76±0·05	12±10	1433	91	1·13±0·09	28±10
1577	93	1·57±0·19	1577	94	1·08±0·08	320±10	1576	95	1·40±0·09	60±12
1717	98	1·85±0·03	1716	98	1·03±0·08	0±15	1716	99	1·53±0·13	46±10
1890	103	1·87±0·04	1890	103	1·02±0·06	0±15	1888	104	1·18±0·07	48±12
PKS 2356−61 (23−64)										
0	—	23·0±1·6	0	—	0·26±0·1	—	0	—	1·13±0·1	360
525	146	2·8±0·1	524	147	1·02±0·08	278±6	523	148	0·59±0·09	100±10
641	140	5·7±0·1	640	141	0·84±0·05	16±4	638	142	0·05±0·04	63±4
797	132	5·8±0·14	795	133	0·26±0·15	351±35	792	134	0·33±0·15	128±25
945	128	5·3±0·2	943	129	0·22±0·04	12±12	941	130	0·24±0·04	118±10
1100	124	4·5±0·1	1098	124	0·20±0·06	10±16	1095	126	0·27±0·04	199±11
1251	119	2·94±0·1	1249	120	0·06±0·06	345±20	1245	121	0·46±0·14	300±20
1394	115	2·01±0·11	1392	116	0·17±0·04	138±12	1389	117	0·45±0·04	310±8
1543	111	4·3±0·11	1540	112	0·37±0·04	204±8	1537	113	0·38±0·04	354±8
1659	107	5·9±0·1	1657	108	0·34±0·18	180±30	1654	109	0·27±0·07	348±28
1777	103	6·3±0·1	1775	103	0·21±0·12	158±16	1772	105	0·53±0·04	301±12
1897	99	6·4±0·1	1896	99	0·20±0·04	61±13	1893	101	0·27±0·04	287±15

source but can be significant elsewhere, e.g. if the projected baseline crosses the minor axis during observation. In the present case it has been assumed that the inversion yields the strip brightness distribution in a direction parallel to the mean

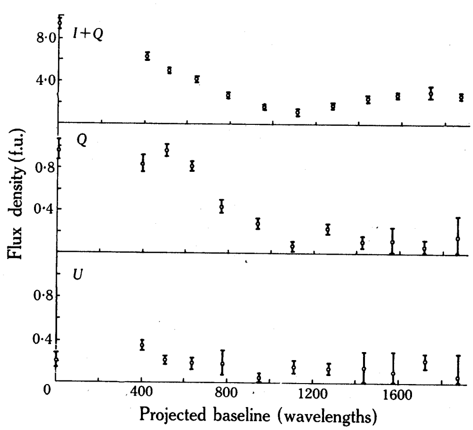

Fig. 3.—Visibility functions for $I+Q$, Q, and U for the source PKS 0043−42. The values for zero spacing correspond to the single-dish observations of Table 1.

position angle of the projected baseline. In the figures this has been designated the scan position angle. For PKS 2356−61 the rotation of the source in relation to the projected baseline was significant. Ekers (1967) has suggested that the source consists of a number of small-diameter components distributed along the major axis. Hence, in the inversion it was assumed that rotation merely caused a variation of projected baseline without affecting the shape of the effective strip brightness distributions.

Values for amplitude and phase at projected baseline intervals of 200 wavelengths were interpolated from the measurements, and the one-dimensional brightness distributions were derived for $I+Q$, U, and Q for a 17′ arc scan. No correction for the tapering of these distributions by the primary beam shape (Fig. 2(*a*)) has been made. To reduce the side lobe responses produced by the cutoff of the Fourier transform at the maximum spacing, further smoothing was generally carried out with a 1′ Gaussian beam. Apart from any additional loss of resolution produced by source rotation, the overall beamwidth then corresponds to 1′·2 arc. Figure 4 illustrates the resulting distributions of $I+Q$, Q, and U for PKS 0356+10. The corresponding distributions of the polarized flux $(U^2+Q^2)^{\frac{1}{2}}$ and the position angle of polarization $0\cdot5\tan^{-1}(U/Q)+\theta$ (integrated polarization) are given in Figure 7. The observations with parallel feeds were also inverted as a check on the plausibility of the assumed phases and on any systematic errors due to source rotation.

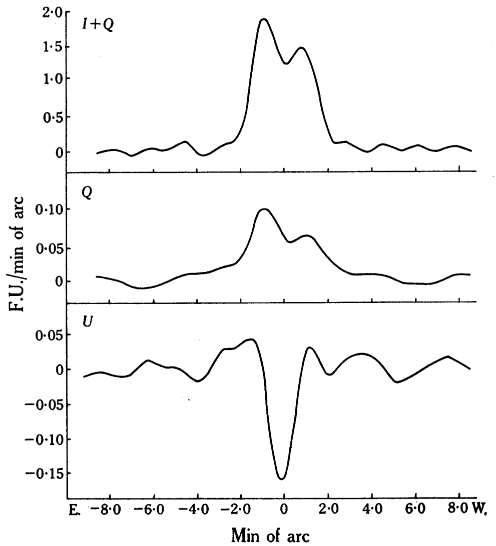

Fig. 4.—Restored strip brightness distributions of $I+Q$, Q, and U for the source PKS 0356+10. The results have been smoothed with a Gaussian function of 1′ arc width to half-intensity points.

Table 3 indicates how the absolute phases were obtained for each source. It also presents a summary of the results of the inversions.

Figures 5–18 illustrate the derived brightness distributions. For each source the one-dimensional strip brightness distribution of the polarized radiation $(U^2+Q^2)^{\frac{1}{2}}$ is plotted together with that of $I+Q$. Accompanying each brightness distribution is the variation of the position angle of polarization. The appended position angle scale has been corrected for ionospheric Faraday rotation. The "modified axis" corresponds to the position angle of the major axis after allowance for the Faraday rotation from zero wavelength to 21·2 cm, as determined from measurements of the integrated radiation (Gardner and Davies 1966*a*). If the changes in Faraday rotation and spectral index over a source are insignificant, the modified axis is of help in visualizing the orientation of the magnetic field in the source relative to its major axis.

TABLE 3

SUMMARY OF CONCLUSIONS AT 21·2 CM

PKS Source No.	Derivation of Phase*	Distribution of Polarization	Angle between Polarization Components† (°)	Intrinsic Angle Minus P.A. Major Axis‡ (°)	Peak Polarization (%)
0043−42	E	Single	0 ± 10	0 ± 3	20
0106+13	S	Double	6	71 ± 9	7 (E.) 11 (W.)
0356+10	S	Triple ?	50 ± 20	25 ± 12	~10
0518−45	F	Double+ Bridge	0 ± 2 ~40	-1 ± 5	8 (E.) 11 (W.) ~4
0618−37	E	Single	20 ± 20	-15 ± 5	13
0945+07	F	Triple ?	V	70 ± 12	12 (E.) 7 (W.)
1216+06	F	Double	0 ± 20	9 ± 8	15 (E.) 13 (W.)
1322−42	F[b] S[c]	Double	20 (V)	100 ± 4	10 (E.) 7 (W.)
1559+02	F	Double	V	66	9 (E.) 3 (W.)
1648+05	F	Single ?§	70 ?	-72 ± 4	1·5 (E.) 0·5 ? (W.)
1717−00	F	Double	V	-8 ± 8	2·5 (E.) 11 (W.)
2152−69	E[a]	Double	~40 (V)	-64 ± 12	9 10
2356−61	E[a]	Double‖	50 ± 10	-125 ± 6	5 8

* E, from Ekers (1967) model; F, Fomalont (1967*a*, 1967*b*) observations; S, Seielstad (1967) model. E[a], Ekers model, sign of calculated phases unknown; F[b], Fomalont observations for scans close to east–west line; S[c], Seielstad model for scans close to the minor axis.

† V, varies over source.

‡ See Table 1.

§ There is some evidence for polarization of the western component.

‖ With additional components (Ekers 1967).

Calculated estimates of the errors introduced into the distribution of polarized radiation $(U^2+Q^2)^{\frac{1}{2}}$ by receiver noise are indicated by the error bars situated to the left of each scan. A better indication of the uncertainties involved is provided by the baseline variations in directions adjacent to the source. They reflect errors due to noise, errors in interpolation, and errors in the assumed phases. Systematic effects due to the rotation of the source during the observations are more difficult to assess since they depend on the two-dimensional brightness distributions.

(*b*) *Individual Sources*

PKS 0043−42: Figure 5

The polarization is distributed over the whole source and shows no structure when scanned with the 1′ ·2 beam. The direction of polarization is constant to within ±10° over the source. The constancy of this direction and the lack of depolarization

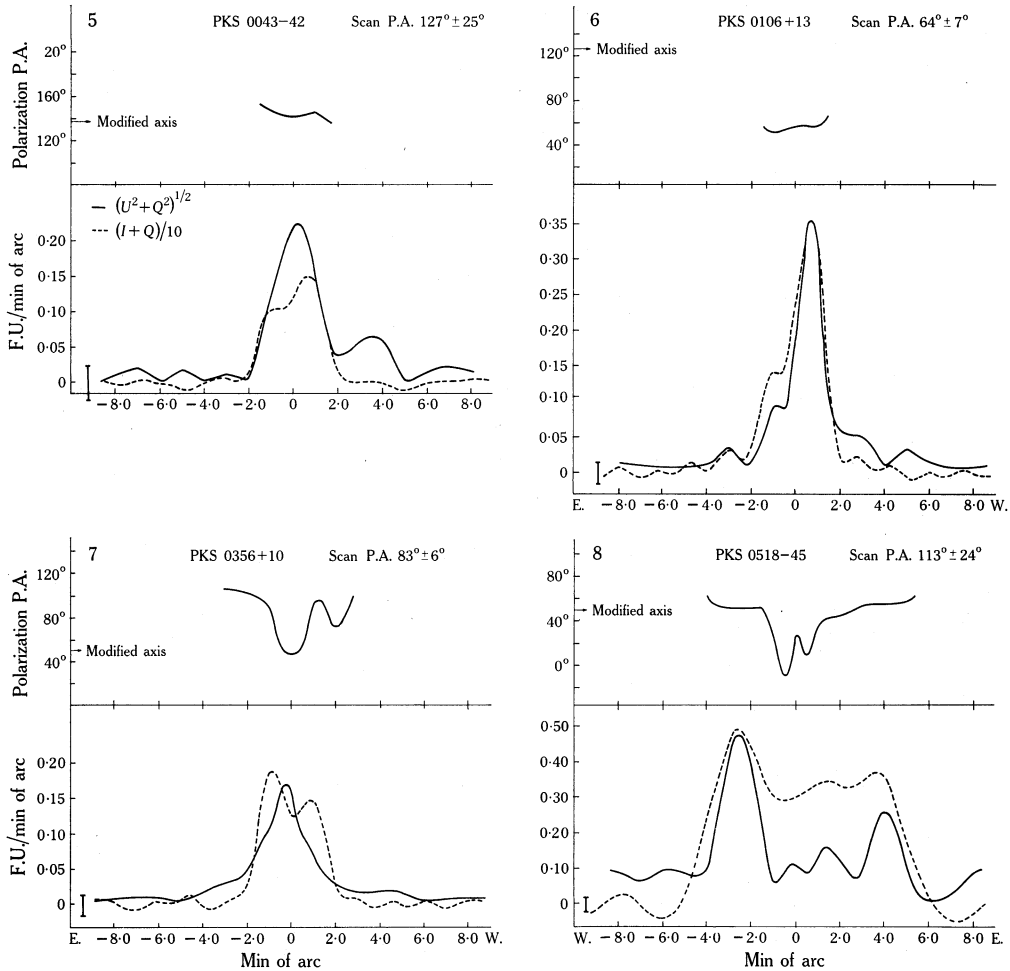

Figs. 5–18.—Strip brightness distributions for the total radiation (actually $(I+Q)/10$) (dashed line), the polarized flux density $(U^2+Q^2)^{\frac{1}{2}}$ (full line), and the direction of polarization. The effective resolution is 1′·2 by 20′. The flux densities have not been corrected for the shape of the primary beam.

shown by the single-dish observations (Gardner and Davies 1966*b*) both imply simple polarization structure. The intrinsic angle of polarization is similar to the position angle of the major axis (136°) and suggests that the projected magnetic field over a major portion of the source is aligned almost perpendicular to its major axis. In this respect the source is similar to 3C452 (Seielstad 1967).

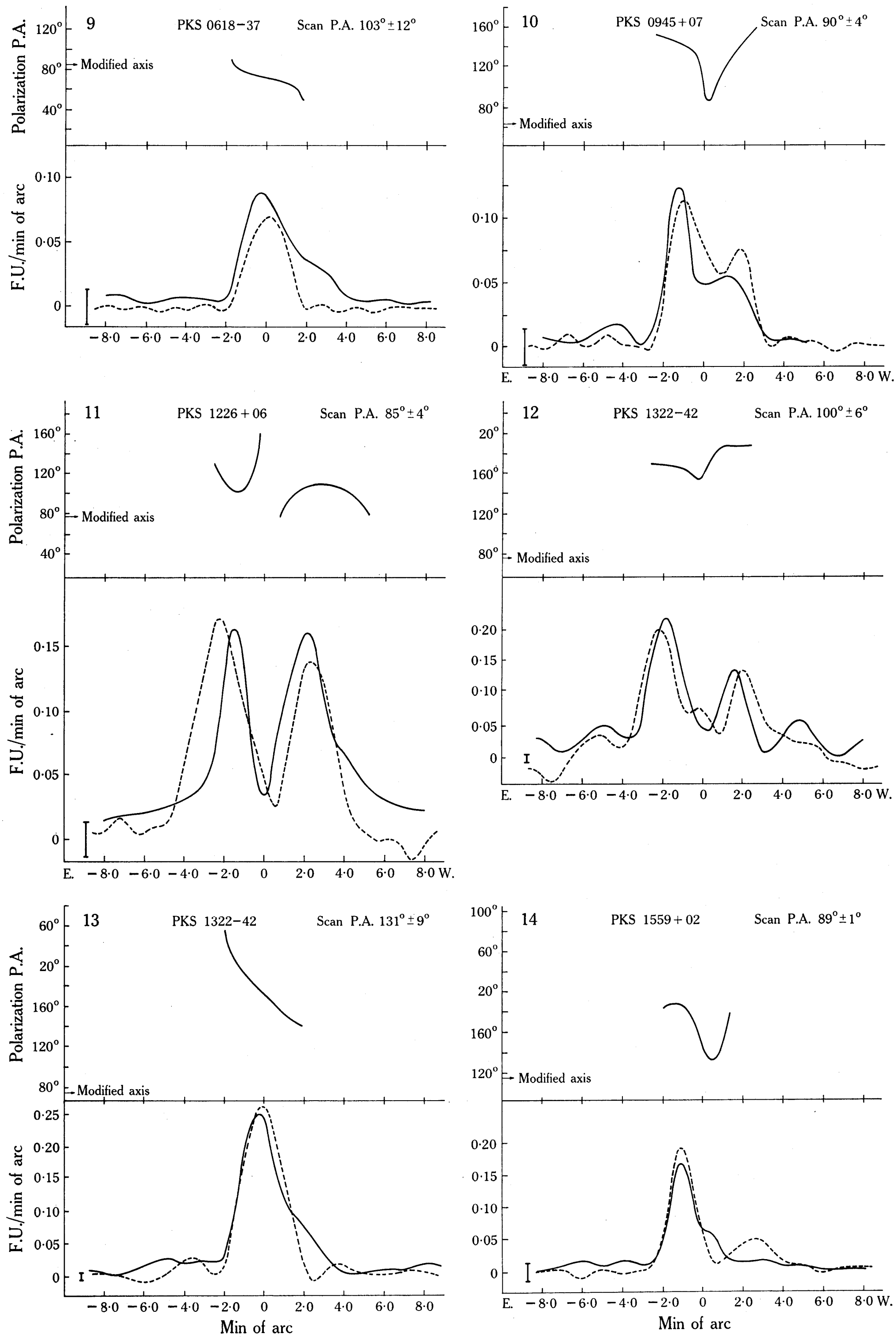

Figs. 5–18 (*continued*)

PKS 0106+13 (3C 33): Figure 6

Both components of the source show polarization; the more intense one has a peak polarization of about 9%, the other about 6%. The position angle of polarization is similar for both cases. These results simulate those of Seielstad (1967) at 10·6 cm. It would appear that the projected magnetic field is almost parallel ($\pm 25°$) to the major axis.

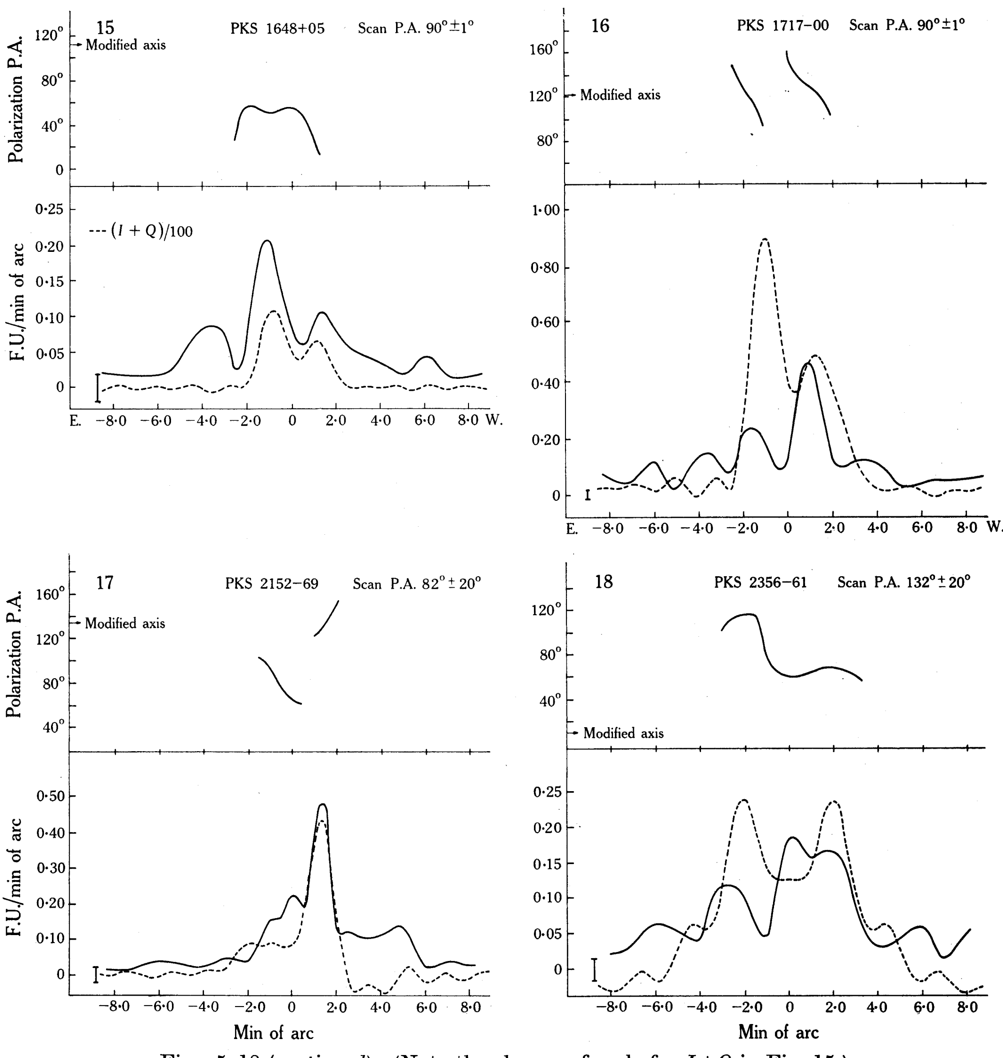

Figs. 5–18 (*continued*). (Note the change of scale for $I+Q$ in Fig. 15.)

PKS 0356+10 (3C 98): Figures 4 and 7

Although both components are polarized in similar directions there is an unresolved core between them which is polarized at an angle differing by about 45°. This is most clearly shown by the variation of U in Figure 4. This result conflicts with the conclusions of Seielstad (1967). However, the apparent difference is probably due to the limited number of antenna spacings available to Seielstad.

PKS 0518—45 (Pictor A): Figure 8

The source was not observed at maximum spacing, so the results have been smoothed with a 2′ Gaussian beam. In accordance with Seielstad (1967) at 10·6 cm, most of the polarized radiation originates in two compact regions at opposite extremities of the source. The peak polarizations are about 5% and 8% for the western and eastern components respectively. The intervening "bridge", on the other hand, shows some polarization of probably 2% and certainly less than 5%. There is some indication of quite complex structure in the distribution of degree and direction of polarization within the bridge. This is not evident in Seielstad's model, since he confines the polarization to the extremities. His conclusion appears to be a consequence of the limited number of antenna separations used. Perhaps for the same reason the 10·6 cm results indicate that the directions of polarization of the two components differ by 72°. The present 21·2 cm results suggest that the two components are polarized approximately parallel to one another. However, the directions of polarization at 6 cm (Broten *et al.* 1965; Morris and Whiteoak 1968) show differences of 50° and 43°±6° respectively, and it appears that the rotation measures of the two components differ by about 16 rad/m². The projected magnetic field in the two extreme components is approximately perpendicular to the major axis.

PKS 0618—37: Figure 9

This source has polarization characteristics similar to PKS 0043—42. The polarization is distributed over a large fraction of the source and has a peak value of about 10%; approximately the single-dish value. Therefore, the characteristics of the polarization are adequately described by the integrated values (Table 1), which imply that the projected magnetic field is almost orthogonal to the major axis (within 15°).

PKS 0945+07 (3C 227): Figure 10

Fomalont (1967*b*) has suggested that the source consists of three components. All components are polarized but the position angle of polarization of the central component differs from that of the outer components by about 50°. In this respect the source is similar to PKS 0356+10 (3C 98). There is apparently a change in direction of polarization over the face of the western component. The integrated values (Gardner and Davies 1966*b*) show depolarization, and the magnetic field structure must be complex.

PKS 1226+06 (3C 270): Figure 11

Both components show quite high (7–10%) peak polarizations and similar directions of polarization. It appears that the angular sizes of the two polarized regions differ significantly at 21·2 cm. At 10·6 cm, on the other hand, the models of Seielstad (1967) indicate identical angular diameters; the difference may be due to depolarization at the outer edge of the eastern component at the longer wavelength. Any associated changes in polarization direction must be too small to be shown. The projected magnetic field is approximately perpendicular to the major axis (within 25°).

PKS 1322−42 (Central Component of Centaurus A): Figures 12 and 13

The scan at P.A. 100° (Fig. 12) shows the polarization of the two main components of the source. The baseline variations indicate quite large errors but the integrated polarization of the components amounts to $6\cdot5\% \pm 1\cdot5\%$ and $3\cdot7\% \pm 1\cdot5\%$ for the eastern and western components respectively. Their directions of polarization differ by 20° in the sense ΔP.A.(W.–E.) = 20°. This is similar to the 10·6 cm results of Seielstad (1967), but at 6 cm the sense is reversed, since ΔP.A.(W.–E.) = −43° (Morris and Whiteoak 1968) or ΔP.A.(W.–E.) = −28° (Cooper, Price, and Cole 1965). These variations with wavelength are mirrored in the changing ratio of the integrated percentage polarization of the two components. At 21·2 cm a ratio of almost two is indicated; at 10·6 cm the ratio is about four, and at 6 cm wavelength the ratio is between six and eight.

The scan in the direction of the minor axis (Fig. 13) shows the rapid variation in direction of polarization previously pointed out by Seielstad (1967). In view of this variation, some of the difference in Faraday rotation between the two components of the source may be due to variations in spectrum over the eastern source.

The intrinsic polarization angle (Table 1), if physically significant for a source with such polarization complexities, indicates that on the average the projected magnetic field direction is within 10° of the orientation of the major axis. The details are clearly very complicated, and more data are needed.

PKS 1559+02 (3C 327a): Figure 14

The present observations indicate that most of the polarized radiation arises in the more intense eastern component. The peak polarization in the 1′·2 by 20′ beam is about 8%.

PKS 1648+05 (Hercules A): Figure 15

At 21·2 cm the integrated polarization of this source is only 0·9% and the observations are consequently subject to large errors. In agreement with Seielstad (1967) at 10·6 cm, most of the polarized radiation is from the more intense eastern component. The present resolution is not sufficient to estimate the angular extent of this region. This source is of high brightness temperature (Maltby and Moffet 1962). The extensive variation of integrated polarization with wavelength (Gardner and Davies 1966*b*) suggests the presence of internal depolarization.

PKS 1717−00 (3C 353): Figure 16

This source is unusual amongst those studied in that the more intense component shows less polarization. Moreover, both components exhibit a large variation in direction of polarization over their diameters. This unusual behaviour is probably related to the substantial depolarization and to the nonlinear relationship between Faraday rotation and wavelength squared that is so evident in the single-dish observations of Gardner and Davies (1966*a*) and Gardner, Morris, and Whiteoak (1968).

The distribution of polarization agrees with that suggested by Seielstad (1967) in his discussion of the work of Gol'nev and Soboleva (1965).

PKS 2152−69: Figure 17

The observations are not of high quality, since considerable uncertainty exists in the assumed absolute phases. Both components are evidently polarized but at angles differing by about 60°. The structure is complex, since the two components have different spectral indices. In addition, this is the only bright double source associated with a D galaxy for which the integrated polarization decreases between 11 cm and 6 cm (Morris and Whiteoak 1968).

PKS 2356−61: Figure 18

This inversion must be treated as strictly a qualitative result. Polarization is associated with one of the principal components and possibly both.

V. Discussion

Of the 13 sources observed, the results for 10 are sufficiently extensive to provide some evidence of their magnetic field structure. In general the distribution of polarization is complex, since several sources have polarization characteristics that vary from one component to the other. Differences of the intrinsic properties of individual components of a source may represent features of a common mode of evolution which are viewed at different epochs in the manner suggested by Ryle and Longair (1967). In the case of the sources PKS 0356+10, PKS 0945+07, and PKS 1322−42, a series of ejecta may have occurred over a substantial period of time to add to the complexity. However, insufficient data are available to determine whether the variation in direction of polarization is due to changes in magnetic field orientation or merely reflects a variation in Faraday rotation.

From observations of the polarization of integrated radiation, it has been pointed out that sources consisting of multiple components fall into two loosely defined classes (Gardner and Whiteoak 1963). In one class the intrinsic angle of polarization is coincident with the major axis; in the other it is orthogonal. Various explanations have been advanced in terms of the evolution of the sources from one class to the other (Gardner and Davies 1964; Morris and Berge 1964; Gardner and Whiteoak 1966). They suggest that the sources with low brightness temperatures and magnetic fields aligned orthogonal to the direction of component separation are the most evolved. In the present investigation this group contains the cources with particularly simple structure, namely, PKS 0043−42, PKS 0518−45, PKS 0618−37, PKS 1226+06, Fornax A, 13–33, and 3C 452 (see Gardner and Whiteoak 1966; Seielstad 1967). The southernmost of the outer components of Centaurus A (Cooper, Price, and Cole 1965) may also fall in this group. We suggest that the highly ordered magnetic fields in these sources may be a consequence of rotation about their major axes. In the last stages of evolution, when the connection of the ejected plasma with the parent galaxy is broken and the internal motions of the plasma in the axial direction have been damped, the rotation that existed in the embryonic stages of the explosion must still persist to conserve angular momentum.

In this way the magnetic lines may be drawn into closely wound helices, and in projection will appear to be aligned perpendicular to the major axis. This idea follows naturally from the theory of Piddington (1966). Any compression of the intergalactic medium will assist in the alignment of the magnetic lines (Gardner and Whiteoak 1966). When viewed along its major axis a single or core–halo source may be visible in which the magnetic lines form tightly wound spirals. The electric vectors of the radiation will be directed radially in projection and the net polarization will be small. On the other hand, the young sources of high brightness temperature, e.g. PKS 0106+13, PKS 1648+05, Centaurus A (central component), and possibly the quasi-stellar sources (Sastry, Pauliny-Toth, and Kellermann 1967), will have axially directed magnetic fields, since the axial motions of the explosion will presumably be dominant. Viewed along the major axis, a single or core–halo source will be visible with a projected magnetic field that appears radial and gives rise to circumferentially directed polarization.

VI. Acknowledgments

We are indebted to Mr. V. Radhakrishnan for assistance with the reductions. Dr. B. McA. Thomas and Mr. P. W. Butler of the aerial development group were responsible for the design, construction, and installation of the feeds used. Miss J. Merkelijn rendered invaluable help with the observations and their reduction, and Dr. R. W. Clarke advised on computer programming.

VII. References

Batchelor, R. A., Cole, D., and Shimmins, A. J. (1968).—The Parks interferometer. *Instn Radio Engrs Aust.* (in press).
Broten, N. W., *et al.* (1965).—*Aust. J. Phys.* **18**, 85.
Cole, D. J. (1967).—*Proc. astr. Soc. Aust.* **1**, 30.
Cooper, B. F. C., Price, R. M., and Cole, D. J. (1965).—*Aust. J. Phys.* **18**, 589.
Ekers, R. (1967).—Ph.D. Thesis, Australian National University.
Fomalont, E. B. (1967*a*).—*Publs Owens Valley Radio Observatory* **1**, No. 3.
Fomalont, E. B. (1967*b*).—*Obs. Owens Valley Radio Observatory* No. 7/1967.
Gardner, F. F., and Davies, R. D. (1964).—*Nature, Lond.* **201**, 144.
Gardner, F. F., and Davies, R. D. (1966*a*).—*Aust. J. Phys.* **19**, 129.
Gardner, F. F., and Davies, R. D. (1966*b*).—*Aust. J. Phys.* **19**, 442.
Gardner, F. F., Morris, D., and Whiteoak, J. B. (1968).—Measurements of the linear polarization of radio sources between 11 and 20 cm. *Aust. J. Phys.* (in press).
Gardner, F. F., and Whiteoak, J. B. (1963).—*Nature, Lond.* **197**, 1162.
Gardner, F. F., and Whiteoak, J. B. (1966).—*A. Rev. Astr. Astrophys.* **4**, 245.
von Geyer, H. (1966).—*Frequenz* **20**, 28.
Gol'nev, V. Ya, and Soboleva, N. S. (1965).—*Astr. Zh.* **42**, 694.
Maltby, P., and Moffet, A. T. (1962).—*Astrophys. J. Suppl. Ser.* **7**, 93.
Minnett, H. C., and Thomas, B. McA. (1966).—*IEEE Trans. Antennas Propag.* **AP14**, 654.
Morris, D., and Berge, G. L. (1964).—*Astr. J.* **69**, 641.
Morris, D., Radhakrishnan, V., and Seielstad, G. A. (1964).—*Astrophys. J.* **139**, 551.
Morris, D., and Whiteoak, J. B. (1968).—*Aust. J. Phys.* **21**, 493.
Piddington, J. H. (1966).—*Mon. Not. R. astr. Soc.* **133**, 163.
Roberts, J. A., and Komesaroff, M. (1965).—*Icarus* **4**, 127.
Ryle, M., and Longair, M. S. (1967).—*Mon. Not. R. astr. Soc.* **136**, 123.
Sastry, Ch. V., Pauliny-Toth, I. I. K., and Kellermann, K. I. (1967).—*Astr. J.* **72**, 234.
Seielstad, G. A. (1967).—*Astrophys. J.* **147**, 24.